Journal of Luminescence 197 (2018) 38–46

Contents lists available at ScienceDirect

Journal of Luminescence

journal homepage: www.elsevier.com/locate/jlumin

Luminescent and gas sensor properties of the ZrO_2:Hhpa:Eu^{3+} Hybrid Compound

I.L.V. Rosa[a,*], F.A. Tavares[a], A.P. de Moura[b], I.M. Pinatti[a], L.F. da Silva[c], M.S. Li[d], E. Longo[b]

[a] Federal University of Sao Carlos (UFSCar), Chemistry Department, LIEC, CEP 13565-905 São Carlos, SP, Brazil
[b] Chemistry Institute, LIEC-CMDMC, UNESP, CEP 14800-900 Araraquara, SP, Brazil
[c] Department of Physics, Federal University of São Carlos (UFSCar), CEP 13565-905 São Carlos, SP, Brazil
[d] Physics Institute of Sao Carlos, USP, CEP 13560-970 Sao Carlos, SP, Brazil

ARTICLE INFO

Keywords:
Nanostructures
Luminescence
Hybrid material
ZrO_2
Europium
3-hydroxypicolinamide

ABSTRACT

Luminescent complexes of rare earth have been extensively studied in different fields of research improving the industrial development of these materials for their utilization as electroluminescent displays, catalysts and biomaterials. The interest in rare earth compounds having aromatic ambidental ligands has increased since it was found that they can act as light collectors (antenna effect), thus bypassing the weak absorption of the lanthanides and resulting in highly efficient luminophors. In this work ZrO_2 was prepared by the hydrothermal microwave method (HMM) at 140 °C for 32 min. The hybrid materials was obtained using the previous ZrO_2 dispersed in distilled H_2O, to which was added Eu^{3+} and the 3-hydroxypicolinamide (Hhpa), and then stirred for about 3 h. The materials were analyzed by X-ray diffraction (XRD) and Transmission electron microscopy (TEM). The photoluminescent properties were investigated through their excitation and emission spectra, and gas sensor studies were also performed. It was observed the presence of completely crystalline powders for all materials, and XRD peaks were indexed to the tetragonal phase of ZrO_2 (JCPDS 50-1089). TEM micrographs reveal a spherical nanostructure pattern presenting an average diameter of 4 nm. Excitation and emission spectra revealed the characteristic peaks of the Eu^{3+} transitions. The studies of these powders as gas sensors showed a significative change in the electric resistance for the hybrid material.

1. Introduction

Rare earth luminescent complexes have been utilized in different fields in the last decade. These materials can be used in the fabrication of electroluminescent displays, fluorescent probes, catalysts, as well as biosensors and can be a promising candidate as gas sensors. The luminescent properties of Eu^{3+} complexes are very interesting due to their thin emission bands and their long lifetime. Eu^{3+} ion presents intraconfigurational *4f-4f* transitions which are Laporte forbidden and consequently presents low absorption intensity. The presence of organic ligands, however, can intensify the ability of Eu^{3+} ions emission through the ligand absorption and transfer part of this energy in an energy transfer mechanism called as antenna effect. This phenomenon resulted in various researches and different ligands were used to this purpose. These organic-inorganic hybrid materials have attracted great interest because of their potential applications in different aspects of technology like optical materials or laser systems [1–4].

Nanostructures of zirconium oxide, ZrO_2, have been explored due to their technological importance based on their high hardness, elevated refractive index, optical transparence, chemical stability, low conductivity, high coefficient of thermal expansion, and high resistance to the corrosion [5,6]. These properties provide to ZrO_2 different application in the field of optic [7], solid state electrolytes, gas sensors, and so on [8]. The application of ZrO_2 in the photonic field is already know due to their high performance in wave guide and their efficient thermoluminescent response [9,10]. The properties of ZrO_2 can be influenced by the preparation method, being possible to obtain metastable phases depending on the methodology employed. Microcrystalline ZrO_2 is obtained when prepared at atmospheric conditions and it is obtained as amorphous, monoclinic, tetragonal, and cubic polymorphic phases [11,12]. So, ZrO_2 can be present as three different crystalline structures P21/c monoclinic (bellow 1170 °C), P42/nmc (137) tetragonal (between 1170 and 2370 °C) and Fm3m (225) cubic (up to 2370 °C) [13].

The monoclinic phase (A) is less symmetric than the tetragonal one (B), and is more stable at room temperature. This phase is transformed in the tetragonal one at 1170 °C, but at 2370 °C the cubic phase (C) is formed [14]. The phases obtained at higher temperatures are unstable

* Correspondence to: Federal University of São Carlos, Via Washington Luis Km 235, CEP: 13.565-905 São Carlos, SP, Brazil.
E-mail address: ilvrosa@ufscar.br (I.L.V. Rosa).

https://doi.org/10.1016/j.jlumin.2017.12.046
Received 17 August 2017; Received in revised form 20 December 2017; Accepted 22 December 2017
Available online 24 December 2017

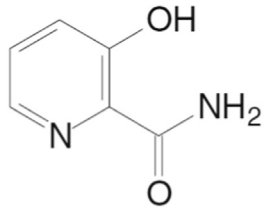

Fig. 1. Molecular structure of the 3-hydroxipicolinamide (Hhpa) ligand.

at room temperature, but these phases are more important for technological applications than the monoclinic one. So, various bivalent and trivalent cationic species like Mg^{2+}, Ca^{2+}, and Y^{3+} are incorporated to the ZrO_2 promoting the obtention of the cubic and tetragonal phases stables at room temperature [15].

Some works reported the doping of ZrO_2 with different rare earths like Er^{3+}, Eu^{3+}, and Sm^{3+} [16–18]. However, few of them focused on the photoluminescent properties of ZrO_2 doped with Eu^{3+} [19–21]. The spectroscopic and magnetic properties of the rare earth ions are responsible for innumerous researches based on these elements. The luminescent spectra of the Eu^{3+} present narrow lines of excitation and emission, due to the electronic transitions inside the unfilled *4f* shell. Also because of the unfilled shell, the ion presents a great number of energy levels, given rise to emission lines that appears in the luminescence spectra from ultraviolet to the infrared, and depends on the kind of matrix they are incorporated. The *4f* orbitals are protected from the environment by *5s* and *5p* ones, so there are weak effects from the ligands field. The f-f transitions are forbidden by Laporte and spin rules, but these rules are broken when the symmetry around this ion is low [22]. The Eu^{3+} is the most studied from the rare earth ions due to it special characteristics. In general, the Eu^{3+} ion presents a more intense luminescence [23]. The characteristic red emission of Eu^{3+} is due to the transitions from the excited $^5D_0$ level to the fundamental ones ^7F_J (J = 0–6) of its $4f^6$ configuration. These characteristics make this ion very useful in illuminations, TV color screen, and displays to diode productions.

The recent interest in study the organic-inorganic hybrid materials is motivated by the presence of their extraordinaire properties which promote their applicability in different field, since this material combine the mutual vantages from the organic and inorganic material [1,24]. Hybrid materials formed with Eu^{3+} and one organic ligand are used to fabricate red luminophors for the obtention of white light emitter diodes (LEDs), since the emission of the white light can be obtained by the incorporation of blue, green, and red luminophors. The organic ligands act as antenna, which increase the luminescent intensity due to the presence of chromophores groups [1,25–29].

The organic compound 3-hydroxipicolinamide (Hhpa), Fig. 1, is an aromatic ligand considered as a model compound that is a component of the virginiamycine S (VS), an hexapeptide which act as an antibiotic that promotes the blocking of the protein synthesis into the bacterial ribosome. The 3-hydroxipicolinil residue absorbs the light and is also responsible for the complexant properties and to the phenomenon of the transference of the protons to the peptide VS. It is believed that the complexation of the species hpa (deprotonated ligand) with the rare

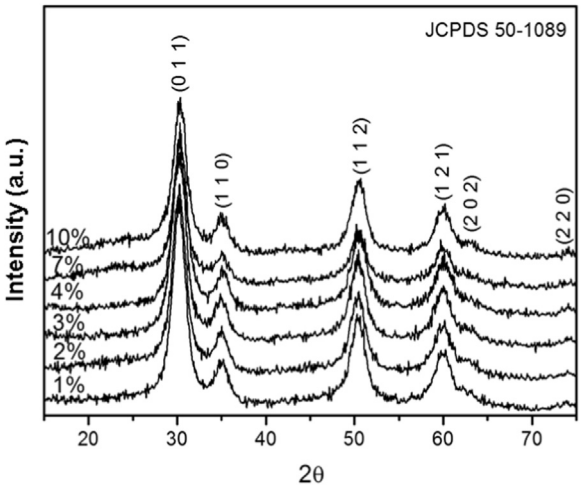

Fig. 3. Powder X-ray diffractograms of the ZrO_2:Hhpa:Eu^{3+} presenting different Eu^{3+} concentration: 1.0%, 2.0%, 3.0%, 4.0%, 7.0%, and 10.0%.

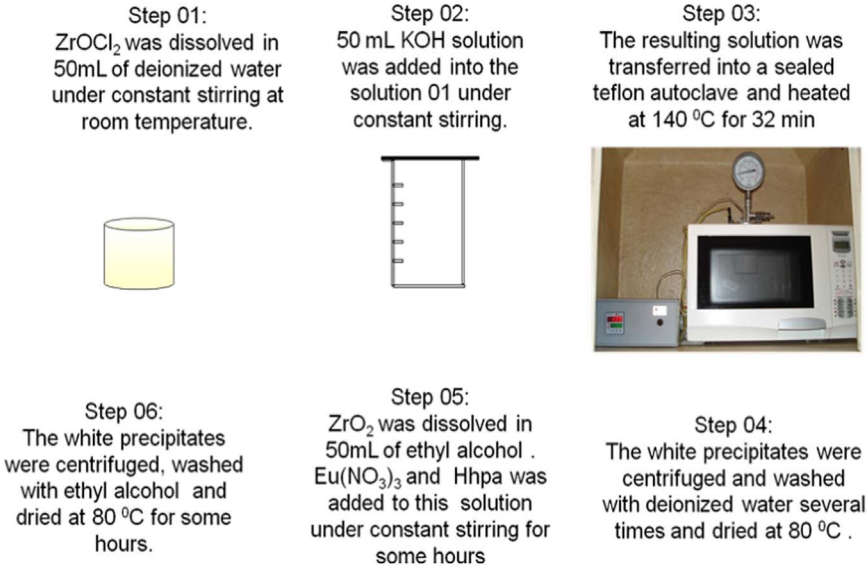

Fig. 2. Experimental procedure for preparation of the samples ZrO_2, ZrO_2:Hhpa:Eu, as well ZrO_2:Bipy:Eu.

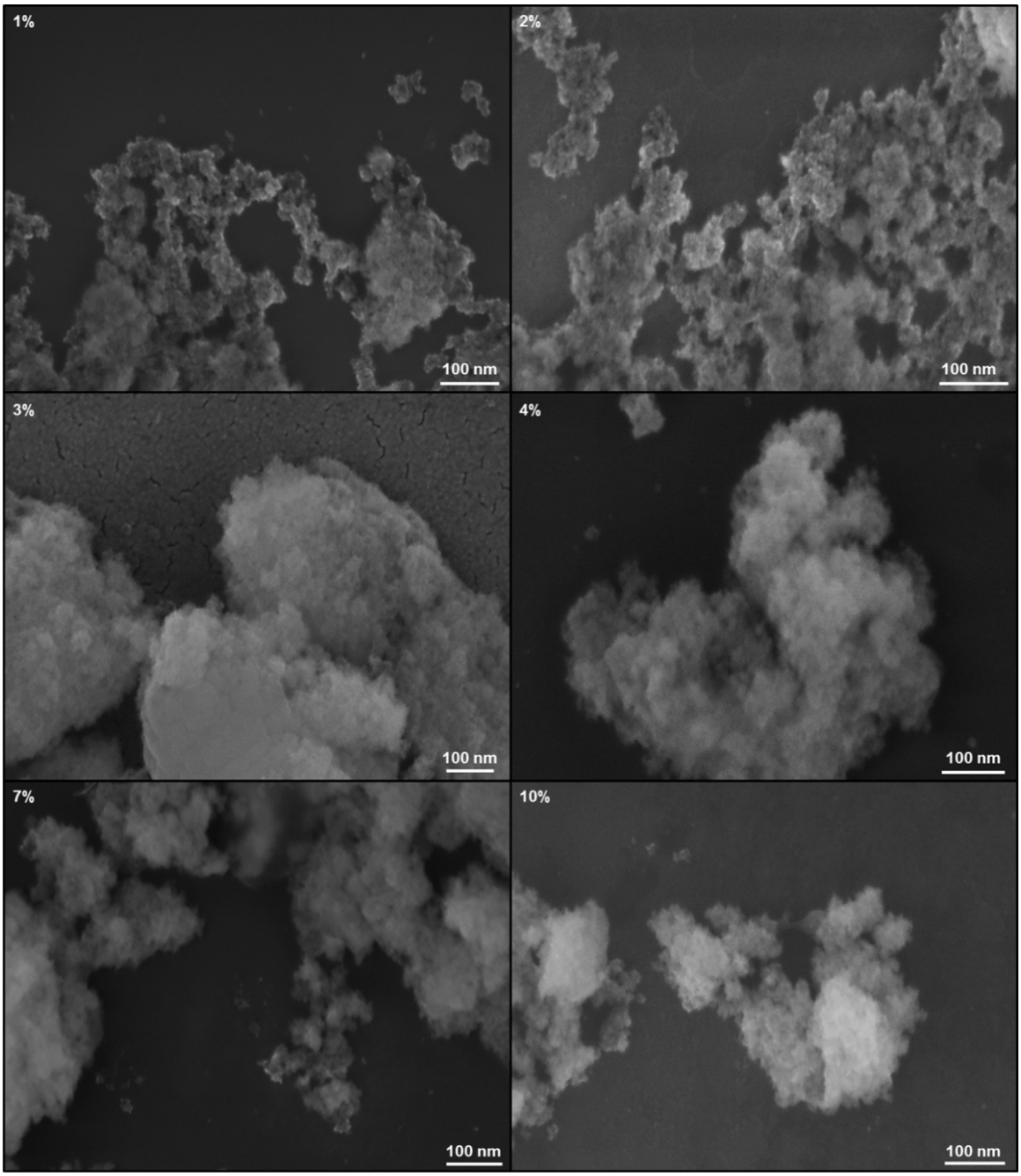

Fig. 4. FE-SEM micrographies of ZrO_2:Hhpa:Eu^{+3} presenting different Eu^{3+} concentration (a) 1.0%, (b) 2.0%, (c) 3.0%, (d) 4.0%, (e) 7.0%, and (f) 10.0%.

alkaline ions occurs through the oxygen from the phenolate group with the participation of the amide from the carboxylic group [11].

In this work ZrO_2 was prepared by the hydrothermal microwave method (HMM) at 140 °C for 32 min. The hybrid materials, ZrO_2:Hhpa:Eu^{3+}, were obtained using the previous ZrO_2 dispersed in distilled water, in which was added 1.0%, 2.0%, 3.0%, 4.0%, 7.0%, and 10.0% in mass of Eu^{3+}, as well as the ligand 3-hydroxypicolinamide (Hhpa). These solutions were stirring for about 3 h, being filtered and washed several times with distilled water and ethanol, and then dried overnight at 60 °C. These samples were analyzed by powder X-ray diffraction (XRD), Scanning Electron Microscopy (SEM) and Transmission electron microscopy (TEM). Their photoluminescent properties were investigated through their excitation and emission spectra. The behavior of these materials was also performed for gas sensors.

2. Experimental section

2.1. Preparation of hybrid material

The samples were prepared according to the steps represented in Fig. 2.

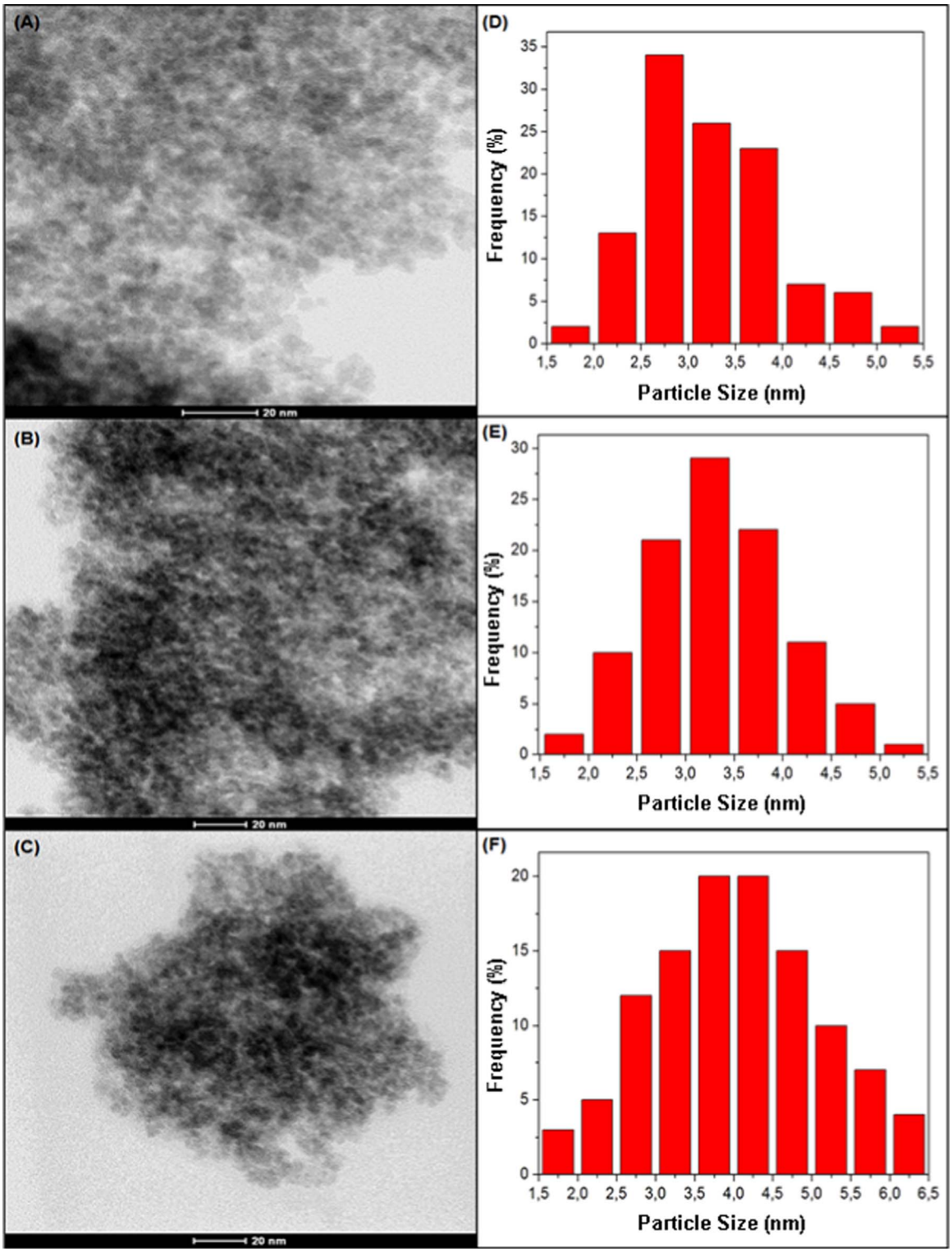

Fig. 5. TEM micrographies and the distribution of the average sizes of the particles for the sample ZrO_2:Hhpa:Eu^{3+} with (A) 1.0%, (B) 2.0%, and (C) 3.0% of Eu^{3+}.

2.2. Structural characterization

Powder X-ray diffraction (XRD) measurements were performed on a Rigaku-D/max 2500 diffractometer (Japan) with graphite-monochromatized Cu Kα radiation (λ = 0.15405 nm). Scan was made from 15° to 75° with a scanning velocity of 2°/min. PL data of the Eu-doped powders were obtained in a Jobin Yvon – Fluorolog III spectrofluorometer under excitation of a 450 W xenon lamp. Luminescence lifetime measurements were carried out as well using a 1940D model spectrophosphorometer coupled to the spectrofluorometer. All the PL measurements were performed at room temperature. The shape and size of the crystals were observed by Field Emission Scanning Electron Microscopy (FE-SEM) through a Carl Zeiss microscope (Model Supra 35) operated at an accelerating voltage of 30 kV and a working distance of 3.7 mm. TEM, at 200 kV measurements were performed using an FEI microscope (model Tecnai G2 F20, FEI, Hillsboro, OR).

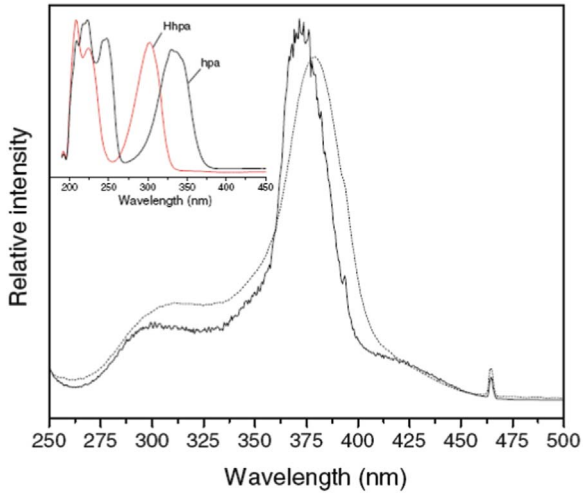

Fig. 6. Excitation spectra of ZrO_2:Hhpa:Eu^{3+} ($\lambda_{Em.}$ = 612 nm) (solid line) at 77 K and at room temperature (dashed line). (Inset: absorption spectra of the ligand Hhpa and hpa species at ethanolic solution).

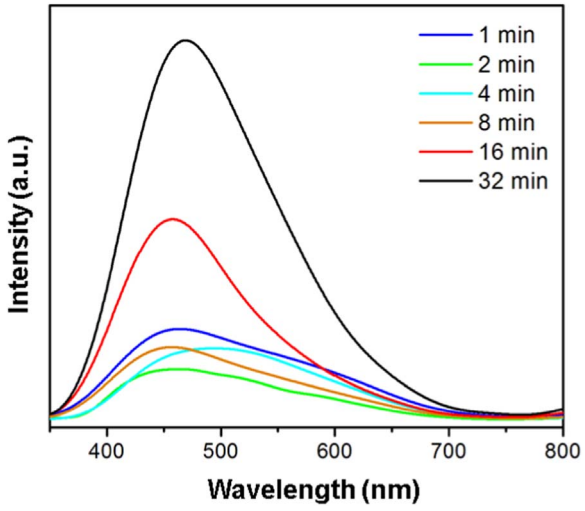

Fig. 7. Emission spectra ($\lambda_{Exc.}$ = 375 nm, room temperature) of the ZrO_2 powders obtained under microwave heat treatment at 140 °C for 1, 2, 4, 8, 16 and 32 min.

3. Results and discussion

The Powder X-ray diffractograms of the ZrO_2:Hhpa:Eu^{+3} presenting different Eu^{3+} concentration: 1.0%, 2.0%, 3%, 4.0%, 7.0%, and 10.0%. XRD of ZrO_2 and ZrO_2:Hhpa:Eu^{3+} are showed at Fig. 3.

The diffractograms presented at Fig. 3 show the same behavior for the species ZrO_2:Eu^{3+}, as well as for the ZrO_2:Hhpa:Eu^{3+} samples presenting different Eu^{3+} concentration: 1.0%, 2.0%, 3.0%, 4.0%, 7.0%, and 10.0%. The presence of Eu^{3+} complexes did not changed the crystallographic behavior of pure ZrO_2 powder. It was noticed that all of materials show the tetragonal phase, and the diffractograms possess the peaks related to this phase at 30.2° (0 1 1), 34,8° (1 1 0), 50.2° (1 1 2), 59.8° (1 2 1), 62.7° (2 0 2), 74.1° (2 2 0), according to the JCPDS (Joint Committee on Powder Diffraction Standards) no 50-1089 from the space group *P42/nmc* [5].

Fig. 4 presents the FE-SEM micrographies of ZrO_2:Hhpa:Eu^{+3} presenting different Eu^{3+} concentrations. This technique was used to observe the morphology of the materials and to identify possible morphological alterations when different organic ligands are employed.

According to these images we can conclude the particles are agglomerated for all of the samples. The particles are nanosized and the presence of the organic ligands did not change significantly the morphology of ZrO_2 powders.

The particle sizes for the samples were evaluated through the TEM analysis, since this technique presents a better resolution than SEM. The TEM micrographies and the distribution of the average sizes of the particles for the sample ZrO_2:Hhpa:Eu^{3+} with 1.0% – (A) and (D), 2.0% – (B) and (E), and 3.0% – (C) and (F) of Eu^{3+} are presented in Fig. 5, respectively. These results show the average particle sizes for the samples of around 2.5–4.5 nm. The difference in Eu^{3+} concentration did not alter significantly these values.

Fig. 6 presents the excitation spectra of ZrO_2:Hhpa:Eu^{3+} ($\lambda_{Em.}$ = 612 nm) (solid line) at 77 K and at room temperature (dashed line). Inset: absorption spectra of the ligand Hhpa and hpa species at ethanolic solution. It is observed a broad excitation band at around 375 nm when the sample was monitored setting the emission at the wavelength of 612 nm. Similar feature was observed for both temperatures used during the acquisition of these excitation spectra [1].

The emission spectra ($\lambda_{Exc.}$ = 375 nm, at room temperature) of the ZrO_2 powders obtained under microwave heat treatment at 140 °C for 1, 2, 4, 8, 16 and 32 min are presented in Fig. 7. These spectra present broad bands covering a large area in the visible range of the electromagnetic spectra indicating that in the photoluminescence emission process are involved different intermediate energy levels in a multiphonon mechanism. The maxima wavelengths for the photoluminescent emission of the samples are centered at around 480 nm, corresponding to the blue emission.

Fig. 8(A) shows the excitation spectra of the ZrO_2:Hhpa:Eu^{3+} (a) 1.0%, (b) 2.0%, (c) 3.0%, (d) 4.0%, (e) 7.0%, and (f) 10.0%; while Fig. 8(B) presents in 2D way the emission spectra of the sample ZrO_2:Hhpa:Eu^{3+}, where the Eu^{3+} concentrations are (a) 1.0%, (b) 2.0%, (c) 3.0%, (d) 4.0%, (e) 7.0%, and (f) 10.0% in weight, using both excitation wavelength of 362 and 393 nm.

It is possible to notice at Fig. 8(A) the Eu^{3+} characteristic excitation bands which maxima are observed at 360, 384, 393 and 464 nm, related to the Eu^{3+} $^7F_0 \rightarrow {}^5D_4$, $^7F_0 \rightarrow {}^5G_1$, $^7F_0 \rightarrow {}^5L_6$ and $^7F_0 \rightarrow {}^5D_2$ transitions, respectively. The large band at around 360 nm are ascribed to the energy transfer from the Hhpa ligand to the Eu^{3+} in the ZrO_2:Hhpa:Eu^{3+} hybrid materials. The antenna effect when the organic ligand is present in ZrO_2 powders is very effective.

The data presented at Fig. 8(B) show the characteristic emission bands of the Eu^{3+} transitions, which maxima intensities are observed at 580 nm ($^5D_0 \rightarrow {}^7F_0$), 593 nm ($^5D_0 \rightarrow {}^7F_1$), 613 nm ($^5D_0 \rightarrow {}^7F_2$), 652 nm ($^5D_0 \rightarrow {}^7F_3$), and 702 nm ($^5D_0 \rightarrow {}^7F_4$) for all of the samples. The samples excited at 362 nm showed more intensity transitions in its emission spectra compared to the samples excited at 394 nm, confirming an efficient energy transfer from the ligand to the Eu^{3+} in the organic-inorganic hybrid materials.

The decay curves of the Eu^{3+} $^5D_0 \rightarrow {}^7F_2$ transition of the samples ZrO_2:Hhpa:Eu^{3+} are presented at Fig. 9 (λem. = 615 and λexc. = 393 nm). The decay curves for all of the samples present biexponential behavior and can be adjusted as the following equation:

$$I = I_1 e^{-(t/T1)} + I_2 e^{-(t/T2)}$$

where, I_1 and I_2 are the intensities for both different decay times (t), T_1 and T_2, respectively. This indicates that the Eu^{3+} ions are localized in at least two different Eu^{3+} sites. As expected for the f-f transitions the lifetime values for these materials were in the microseconds scale, which values are showed in Table 1 [2].

According to the data presented at Figs. 8 and 9, and Table 1, the obtention of the hybrid materials originated from the Eu^{3+} and the ligand 3-hydroxipicolinamide (Hhpa) in the nanometric crystals of the ZrO_2 powders was proved. The study of the photoluminescent properties of these materials shows the Eu^{3+} complex was formed. When the samples were excited at 363 nm the ligand absorbs efficiently the light

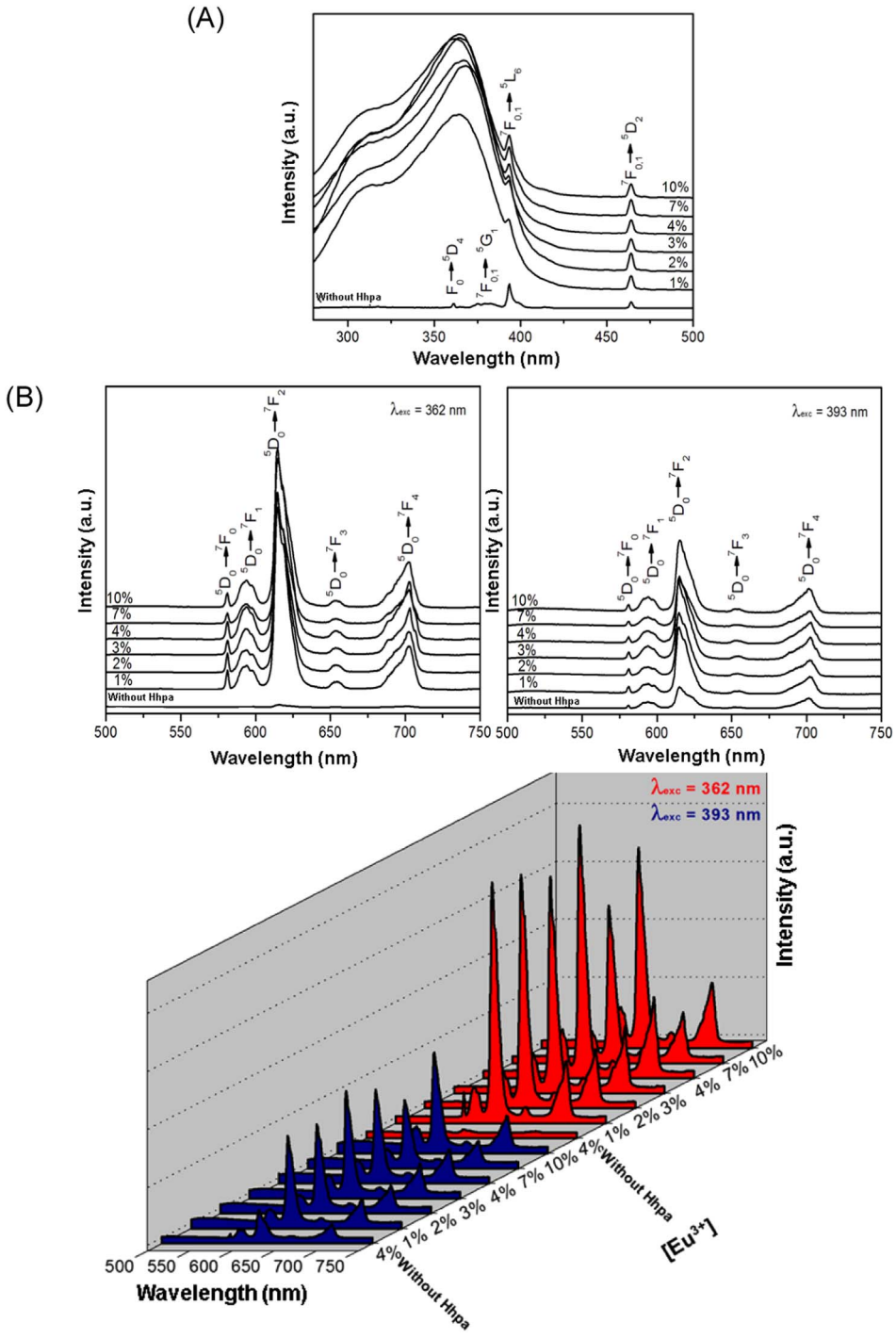

Fig. 8. (A) Excitation spectra of the complex Bipy:Eu^{3+}, ($\lambda_{Em.}$ = 615 nm) at room temperature and ZrO_2:Hhpa:Eu^{3+} presenting different Eu^{3+} concentrations: (a) 1.0%, (b) 2.0%, (c) 3%, (d) 4.0%, (e) 7.0%, and (f) 10.0%. (B) Emission spectra of the samples ZrO_2:Eu^{+3} and ZrO_2:Hhpa:Eu^{+3}, where the Eu^{3+} concentrations are 1.0%, (b) 2.0%, (c) 3.0%, (d) 4.0%, (e) 7.0%, and (f) 10.0% in weight, using both excitation wavelengths, $\lambda_{exc.}$, of 362 and 393 nm.

at this wavelength and transfer part of this energy to the Eu^{3+} that emit their characteristic red emission at 613 nm in a higher intensity when compared to the samples without this organic ligand. The lifetime values of the ZrO_2:Hhpa:Eu^{3+} with different weight % of Eu^{3+} are bi-exponential fitted (Table 1). The sample without the organic ligand presents a lifetime of 0.07 ms while the sample ZrO_2:Hhpa:Eu^{3+} with 2.0% of Eu^{3+} presented a lifetime value of around seven times bigger (0.46 ms) than the sample without the organic ligand. Another finding was that the nanoparticles of ZrO_2 were seen in a spherical pattern and agglomerated through the FE-SEM (Fig. 4) and TEM analysis (Fig. 5). The particles presented sizes of around 3 nm and the difference in the Eu^{3+} concentration did not affect in a significant way the structure, morphology neither the optic properties of these materials.

The measurement of the sample colors were evaluated by the Commission internationale de l'éclairage (CIE) coordinates. The CIE diagram of the ZrO_2 samples under different synthesis conditions are plotted in the CIE chromaticity diagram based on the photoluminescence emission spectra. The CIE diagram is shown in Fig. 10(a –

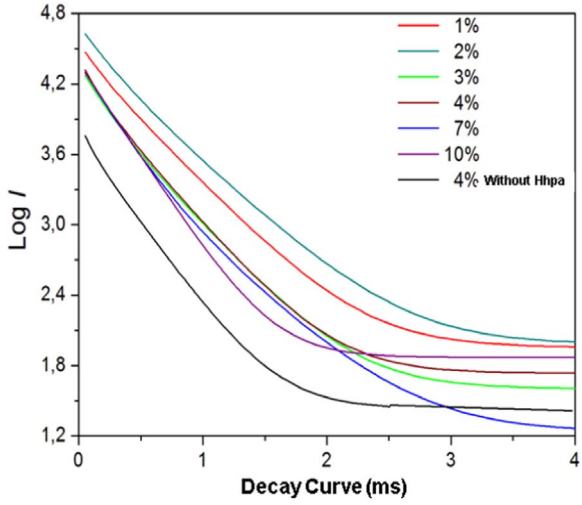

Fig. 9. Intensity versus time (ms) of the $^5D_0 \rightarrow {}^7F_2$ transition of the samples ZrO_2:Hhpa:Eu^{3+} with different % of Eu^{3+}.

Table 1
Lifetime T_1 and T_2 (in ms) of the powders ZrO_2:Eu^{3+} and ZrO_2:Hhpa:Eu^{3+} with different weight % of Eu^{3+}.

% Eu^{3+}	τ_1 (ms)	τ_2 (ms)
1.0%	0.14	0.40
2.0%	0.46	0.19
3.0%	0.17	0.39
4.0%	0.36	0.12
7.0%	0.23	0.55
10.0%	0.22	0.48
4% without Hhpa	0.07	0.29

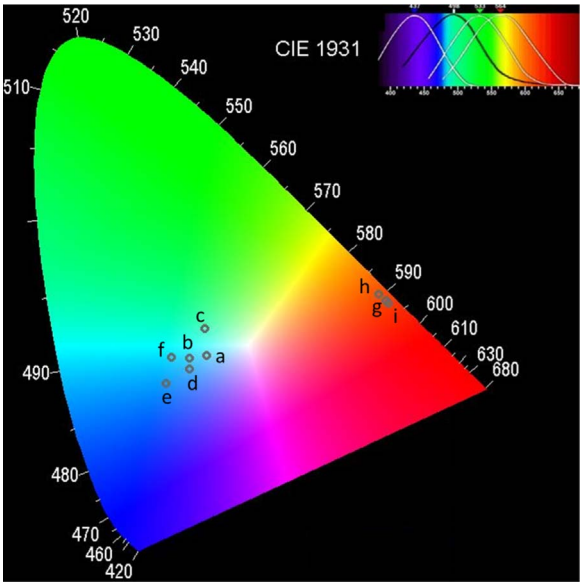

Fig. 10. CIE diagram of the ZrO_2 samples under different synthesis conditions. (a) ZrO_2 1 min, (b) ZrO_2 2 min, (c) ZrO_2 4 min, (d) ZrO_2 8 min, (e) ZrO_2 16 min, (f) ZrO_2 32 min, (g) ZrO_2:Hhpa:3%Eu^{3+}, $\lambda_{exc.}$ = 362 nm, (h) ZrO_2:Hhpa:3%Eu^{3+}, $\lambda_{exc.}$ = 393 nm, and (i) ZrO_2:3%Eu without Hhpa, $\lambda_{exc.}$ = 393 nm.

i), and the respective CIE chromatic coordinates of theses samples are listed in Table 2. The ZrO_2 samples synthesized in different time shows predominant color in the blue-green region of the diagram. The sample ZrO_2 heated for 4 min has the emission in the green region while the

Table 2
CIE chromatic coordinates of the ZrO_2 samples under different synthesis conditions Lifetime T_1 and T_2 (in ms) of the powders ZrO_2:Eu^{3+} and ZrO_2:Hhpa:Eu^{3+} with 3.0 wt% of Eu^{3+}.

Samples	Chromatic coordinates	
	x	y
(a) ZrO_2 1 min	0.282	0.318
(b) ZrO_2 2 min	0.254	0.314
(c) ZrO_2 4 min	0.279	0.361
(d) ZrO_2 8 min	0.255	0.297
(e) ZrO_2 16 min	0.217	0.273
(f) ZrO_2 32 min	0.226	0.316
(g) ZrO_2:3%Eu λ_{exc} = 362 nm	0.571	0.407
(h) ZrO_2:3%Eu λ_{exc} = 393 nm	0.559	0.417
(i) ZrO_2:4%Eu without Hhpa λ_{exc} = 393 nm	0.575	0.403

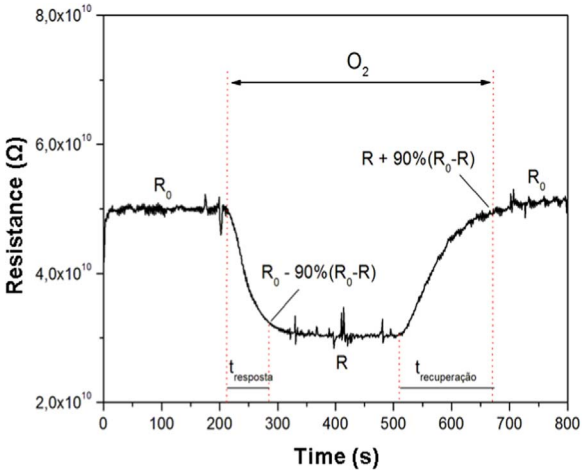

Fig. 11. Illustration of the procedure used to determine the response and recovery time for the representative sample of the material ZrO_2:Hhpa:Eu^{3+} exposed to 50 ppm of O_2 for an operating temperature ($T_{opt.}$) of 300 °C.

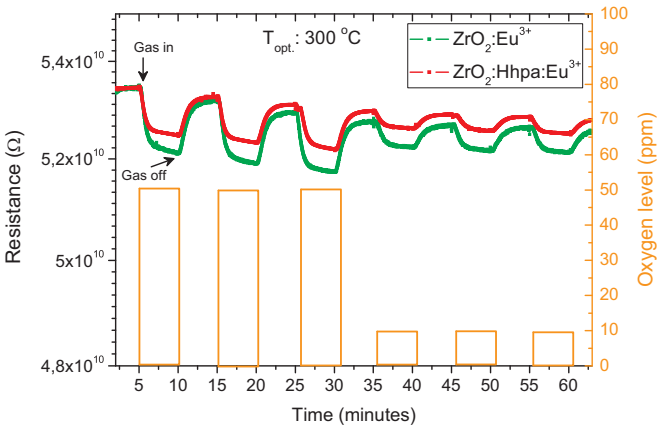

Fig. 12. Electrical resistance of ZrO_2:Eu^{3+} and ZrO_2:Hhpa:Eu^{3+} samples upon exposure to 50 and 10 ppm of O_2, at an operating temperature of 300 °C.

emission of the sample ZrO_2 heated for 16 min is more close to the blue color. The samples ZrO_2:Hhpa:Eu^{3+} doped with Eu^{3+}, on the other hand, presented intense orange color. Both excitation wavelengths (362 and 393 nm) were sufficient to sensitize the Eu^{3+} transitions responsible for their red color. The main intense red color arises specially from the $^5D_0 \rightarrow {}^7F_2$ Eu^{3+} transition observed at 613 nm in the emission spectra. Therefore, the contribution of the blue color to the host lattice

Table 3
Values of response and recovery time for the $ZrO_2:Eu^{3+}$ at 300 °C and ZrO_2:Hhpa:Eu^{3+}, synthesized with 3,0 wt% of Eu^{3+} at 200 and 300 °C, under flux of 10 and 50 ppm of O_2.

Samples	Operating temperature, $T_{opt.}$ (°C)	Response time, t_{res} (s)		Recovery time, t_{res} (s)	
		10 ppm	50 ppm	10 ppm	50 ppm
$ZrO_2:Eu^{3+}$	300	108	102	141	124
ZrO_2:Hhpa:Eu^{3+}	300	126	106	132	129
ZrO_2:Hhpa:Eu^{3+}	200	93	71	140	141

and the red color of the Eu^{3+} are responsible for the dark orange color of these samples. The values presented at Table 2 shows that the sample ZrO_2:3%Eu without Hhpa, $\lambda_{exc.}$ = 393 nm, presented the values (x = 0.575; y = 0.403), which are very close to the commercial phosphor $Y_2O_2S:Eu^{3+}$ values (x = 0.64; y = 0.34), published for the International Standards Chromaticity Coordinates [30]. These results confirm these materials as suitable for applications in several visible lamps, displays and other optical devices.

The study of these materials for application as gas sensors [31–33] was evaluated through the variation of the electric resistance of the nanostructures of ZrO_2, $ZrO_2:Eu^{3+}$ and ZrO_2:Hhpa:Eu^{3+} containing 3% of Eu^{3+} in the presence of different oxygen concentrations (10 and 50 ppm) at 200 and 300 °C. The sensor response (S) was defined as $S = R_{air} / R_{oxygen}$, where R_{air} and R_{oxygen} are the electrical resistances of the sensor upon exposure to dry air and oxygen gas, respectively. The sensor response time (τ_{res}) was defined as the time required for the electrical resistance to reach 90% of the initial value when exposed to oxygen gas. In the same way, the recovery time (τ_{rec}) was defined as the time required for the electrical resistance to recover 90% of the initial value after the oxygen gas flow was switched off.

The velocity of the sensor response was measured through the response time and recovery time. Fig. 11 shows the illustration of the procedure used to determine the response and recovery time for the ZrO_2:Hhpa:Eu^{3+} at 300 °C under O_2 flux of 50 ppm.

The dynamic sensor resistance of ZrO_2:Hhpa:Eu^{3+} samples exposed to oxygen gas is illustrated in Fig. 11. Upon exposure to oxygen gas, the electrical resistance of samples quickly decreased, which is a typical behavior of p-type semiconductors exposed to oxidizing gases [34]. Additionally, the 3-hydroxypicolinamide (Hhpa) addition into the $ZrO_2:Eu^{3+}$ network did not altered the conduction mechanism of the sample, as seen in Fig. 12. The reversible cycles of the sensor curves indicate a stable and reproducible response for both samples. In addition, the sensor response was slightly reduced with the Hhpa addition into the $ZrO_2:Eu^{3+}$, as seen in Fig. 12. The response and recovery times are displayed in Table 3.

The analysis of Figs. 12 and 13 reveals a significant reduction of sensor response with operating temperature from S = 1.02 (300 °C) to S = 1.62 (200 °C), as displayed in Table 3. For temperature below 200 °C, the sample was not sensitivity for this oxygen concentration range. Additionally, even for a lower temperature, the ZrO_2:Hhpa:Eu^{3+} sample exhibit a good reproducibility, and a total reversibility.

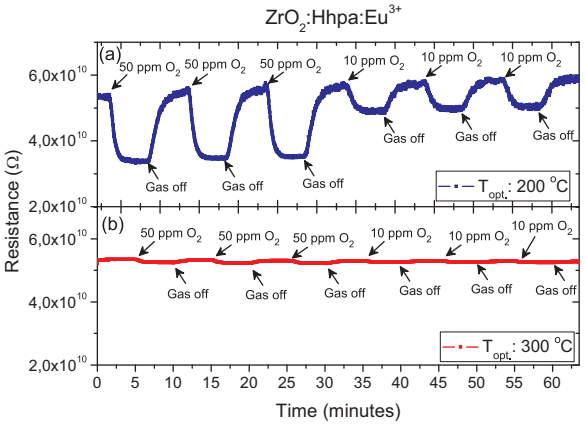

Fig. 13. Electrical resistance of ZrO_2:Hhpa:Eu^{3+} sample upon exposure to 50 and 10 ppm of O_2, at (a) $T_{opt.}$ of 200 °C, and (b) $T_{opt.}$ of 300 °C.

The results above-discussed show clearly that the hybrid ZrO^2:Hhpa:Eu^{3+} compound can be considered as a potential oxygen gas sensor. Nevertheless, the work has demonstrated the multifunctional properties of ZrO_2:Hhpa:Eu^{3+} compound. Further gas-sensing parameters still need to be evaluated, such as, its selectivity to reducing gases, as well as its long-term stability.

4. Conclusions

It was obtained for the first time the completely crystalline powders where XRD peaks were perfectly indexed to the tetragonal phase of ZrO_2 (JCPDS 50-1089). TEM micrographs revealed a spherical nanostructure pattern presenting an average diameter of 4 nm. Excitation and emission spectra revealed the characteristic peaks of the Eu^{3+} transitions. For the first time it is showed here that the ligand plays an important role in transfer energy to Eu^{3+} ion, known as antenna effect, increasing the Eu^{3+} emission intensity of the samples ZrO_2:Hhpa:Eu^{3+} when compared to the species $ZrO_2:Eu^{3+}$. The studies of this materials as gas sensors showed the hybrid ZrO^2:Hhpa:Eu^{3+} compound can also be considered as a potential oxygen gas sensor.

Acknowledgments

The authors thank the support of the Brazilian research financing institutions: grant #2013/07296-2 and grant #2013/23995-8 (São Paulo Research Foundation, FAPESP-CDMF) and grant #132320/2012-6 (CNPq) and CAPES.

References

[1] I.L. Rosa, P.C. Filho, C.R. Neri, O.A. Serra, A.T. de Figueiredo, J.A. Varela, E. Longo, Synthesis and study of the photophysical properties of a new Eu^{3+} complex with 3-hydroxypicolinamide, J. Fluoresc. 21 (2011) 1575–1583.
[2] S. Jianliang, H. Ge, S. Qing, Z. Zhaohong, G. Lei, Nanofibers doped with a novel red-emitting Europium complex: synthesis, characterization, photophysical property and sensing activity toward molecular oxygen, Spectrochim. Acta Part A Mol. Biomol. Spectrosc. 91 (2012) 192–197.
[3] J. Liu, S. Li, W. Liao, Y. Chen, A new europium(III) complex containing a neutral ligand of 2-(pyridin-2-yl)-1H-benzo[d]imidazole: thermal, electrochemical, luminescent properties, Spectrochim. Acta Part A Mol. Biomol. Spectrosc. 107 (2013) 102–107.
[4] K. Sheng, B. Yan, Coordination bonding assembly and photophysical properties of Europium organic/inorganic/polymeric hybrid materials, J. Photochem. Photobiol. A: Chem. 206 (2009) 140–147.
[5] L. Chen, Y. Liu, Y. Li, Preparation and characterization of $ZrO_2:Eu^{3+}$ phosphors, J. Alloy. Compd. 381 (2004) 266–271.
[6] H.D.E. Harrison, N.T. McLamed, E.C. Subbarao, A new family of self-activated phosphors, J. Electrochem. Soc. 110 (1963) 23–28.
[7] G.A. Kourouklis, E. Liarokapis, Pressure and temperature dependence of the raman spectra of zirconia and hafnia, J. Am. Ceram. Soc. 74 (1991) 520–523.
[8] I. Birkby, R. Stevens, Applications of zirconia ceramics, Key Eng. Mater. 122 (1996) 527–552.
[9] Y. Murase, E. Kato, Role of water vapor in crystallite growth and tetragonal-monoclinic phase transformation of ZrO_2, J. Am. Ceram. Soc. 66 (1982) 196–200.
[10] Y. Sorek, M. Zevin, R. Reisfeld, T. Hurvits, S. Ruschin, Zirconia and zirconia-ORMOSIL planar waveguides prepared at room temperature, Chem. Mater. 9 (1997) 670–676.
[11] P. Salas, E.Dl Rosa-Cruz, D. Mendoza-Anaya, P. González, R. Rodríguez,

V.M. Castaño, High temperature thermoluminescence induced on UV-irradiated tetragonal ZrO_2 prepared by sol–gel, Mater. Lett. 45 (2000) 241–245.
[12] K. Erich, C.J. Howard, Zirconia Engineering Ceramics: Old Challenges – New Ideas, (1998).
[13] C.J. Dalmaschio, Modificação Superficial de Óxidos: Proposta de um modelo simples e sua aplicação em sistema alumina-zircônia, in: Chemistry, Federal University of São Carlos, São Carlos, 2008, p. 77.
[14] A.E. Bohé, J. Andrade-Gamboa, D.M. Pasquevich, A.J. Tolley, J.L. Pelegrina, Microstructural characterization of ZrO_2 particles prepared by reaction of gaseous $ZrCl_4$ with Fe_2O_3, J. Am. Ceram. Soc. 83 (2000) 755–760.
[15] R.C. Garvle, Stabilization of the tetragonal structure in zirconia microcrystals, J. Phys. Chem. 82 (1978) 218–224.
[16] E. De la Rosa-Cruz, L.A. Diaz-Torres, P. Salas, R.A. Rodríguez, G.A. Kumar, M.A. Meneses, J.F. Mosiño, J.M. Hernández, O. Barbosa-García, Luminescent properties and energy transfer in ZrO_2:Sm^{3+} nanocrystals, J. Appl. Phys. 94 (2003) 3509–3515.
[17] A. Patra, C.S. Friend, R. Kapoor, P.N. Prasad, Upconversion in Er^{3+}:ZrO_2 nanocrystals, J. Phys. Chem. B 106 (2002) 1909–1912.
[18] A. Gedanken, R. Reisfeld, E. Sominski, O. Palchik, Y. Koltypin, G. Panczer, M. Gaft, H. Minti, Sonochemical preparation and characterization of europium oxide doped in and coated on ZrO_2 and yttrium-stabilized zirconium (YSZ), J. Phys. Chem. B 104 (2000) 7057–7065.
[19] Y. Al-Khatatbeh, K.K.M. Lee, B. Kiefer, Phase relations and hardness trends of ZrO_2 phases at high pressure, Phys. Rev. B 81 (2010).
[20] S. Shukla, S. Leal, Phase stabilization in nanocrystalline zirconia, Rev. Adv. Mater. Sci. 5 (2003) 117–120.
[21] S.F. Wang, F. Gu, M.K. Lü, Z.S. Yang, G.J. Zhou, H.P. Zhang, Y. Zhou, S.M. Wang, Structure evolution and photoluminescence properties of ZrO_2:Eu^{3+} nanocrystals, Opt. Mater. 28 (2006) 1222–1226.
[22] T.S. Martins, P.C. Isolani, Terras raras: aplicações industriais e biológicas, Quim. Nova 28 (2005) 111–117.
[23] F.A. Sigoli, H.F. Brito, M.J. Jr, M.R. Davolos, Luminescence of Eu(III) b-diketone complex supported on q functionalized macroporous silica matrix, Int. J. Inorg. Mater. 3 (2001) 755–762.
[24] Q.M. Wang, B. Yan, A novel way to prepare luminescent terbium molecular-scale hybrid materials: modified heterocyclic ligands covalently bonded with silica, Cryst. Growth Des. 5 (2005) 497–503.
[25] K. Clays, M.D. Giambattista, A. Persoons, Y. Engelborghs, A. Fluorescence, Lifetime study of virginiamycin S using multifrequency phase fluorometry, Biochemistry 30 (1991) 7271–7276.
[26] J. Yang, Z. Li, Y. Xu, Y. Wang, Zirconia-based luminescent organic-inorganic hybrid materials with ternary europium (III) complexes bonded, Opt. Mater. 55 (2016) 78–82.
[27] Z. Li, P. Li, Q. Xu, H. Li, Europium(III)-B-diketonate complex-containing nanohybrid luminescent pH detector, Chem. Commun. 51 (2015) 10644–10647.
[28] H. Li, M. Li, Y. Wang, W. Zhang, Luminescent hybrid materials based on laponite clay, Chemistry 20 (2014) 10392–10396.
[29] J. Feng, H. Zhang, Hybrid materials based on lanthanide organic complexes: a review, Chem. Soc. Rev. 42 (2013) 387–410.
[30] R.F. Gonçalves, M.J. Godinho, A.P.A. Marques, M.R.C. Santos, I.L.V. Rosa, E. Longo, M.S. Li, J.L.S. Sa, L.S. Cavalcante, Structure, morphology, and optical properties of $(Ca_{1-3x}Eu_{2x})WO_4$ microcrystals, Electron. Mater. Lett. 11 (2015) 193–197.
[31] J.L.G. Fierro, Metal Oxides: Chemistry and Applications, (2006).
[32] P.H. Suman, Caracterização de nanoestruturas de óxido de estanho como sensores de gás, in: Chemistry, Universidade Estadual Paulista Júlio de Mesquita Filho, Araraquara, 2012, p. 111.
[33] D. Berger, Efeito da Pressão na Obtenção e nas Propriedades óTicas e Sensoras de Filmes Finos à Base de SnO2 Com a Adição de ZnO, in: Chemistry, Universidade Estadual Paulista Júlio de Mesquita Filho, Araraquara, 2013, p. 104.
[34] L.F. da Silva, V.R. Mastelaro, A.C. Catto, C.A. Escanhoela, S. Bernardini, S.C. Zílio, E. Longo, K. Aguir, Ozone and nitrogen dioxide gas sensor based on a nanostructured $SrTi_{0.85}Fe_{0.15}O_3$ thin film, J. Alloy. Compd. 638 (2015) 374–379.